Soft Matter

Accepted Manuscript

ROYAL SOCIETY OF CHEMISTRY

www.rsc.org/softmatter

Journal Name

ARTICLE

The Application of Low Frequency Dielectric Spectroscopy to Analyze Electrorheological Behavior of Monodisperse Yolk-Shell SiO_2/TiO_2 Nanospheres

Received 00th January 20xx,
Accepted 00th January 20xx

DOI: 10.1039/x0xx00000x

www.rsc.org/

Xiaosong Guo, Yulu Chen, Dong Li, Guicun Li, Meng Xin, Mei Zhao, Chen Yang, Chuncheng Hao*, Qingquan Lei

Monodisperse the SiO_2/TiO_2 yolk-shell nanospheres (YSNS) with different size of SiO_2 core were fabricated and adopted as dispersing materials for electrorheological (ER) fluids to investigate the influence of gradual structural change of disperse particles on ER properties. The results showed that the ER performance of the YSNS-based ER fluid prominently enhanced with the decrease of SiO_2 core size, which were attributed to the enhancement of electric field force between YSNS. Combining with the analysis of dielectric spectroscopy, it was found that the increase of permittivity at low frequency (10^{-2}-10^{0} Hz) was due to the increase of polarized charges caused by secondary polarization (P_{sp}). Moreover, the number of P_{sp} closely related to the distributing change of polarized particles in ER fluid, was a critical factor to assess the ER performance. Additionally, a parameter K (the absolute value of slope of permittivity curves at 0.01 Hz) could be utilized to characterize the efficiency of structural evolution of polarized particles in ER fluid. Compared with the ER performance, it could be concluded that the value of $\Delta\varepsilon'_{(100Hz\text{-}100kHz)}$ just demonstrated the initial intensity of the interface polarization in the ER fluid as the electric field was applied, which ignored distributing evolution of polarized disperse particles in ER fluid. The polarizability $\Delta\varepsilon'_{(0.01Hz\text{-}100kHz)}$ obtained in the frequency range of 10^{-2}-10^{5} Hz should be more suitable for analyzing the system of ER fluid. The relationships between polarizability of disperse particles, parameter K and ER properties were discussed in detail.

Introduction

Electrorheological (ER) fluid, a kind of smart field-responsive suspension with electrically tunable rheology, consists of polarized nanoparticles or microparticles as a disperse phase and insulating oil as a dispersing medium.[1-4] On exposure to an electric field, the suspended particles are polarized and attracted to each other to form a chain structure between the electrodes.[5-6] These fluids have attracted considerable attention in various fields because of their distinguishing features, such as low power consumption, fast response time, reversibility, and simple mechanics.[7-11] However, until now, there are still several limitations for commercialization of ER fluids because of relatively low polarization force.[12-14] In order to overcome the poor ER effect, many efforts have been made to improve the ER performance, such as doping ions, changing the morphology, designing complex structure.[15-18] In addition, the mass of the disperse material often leads to sedimentation problems, which greatly reduces the ER efficiency by disturbing the formation of the fibril-like structures. To overcome this limitation and facilitate the commercialization, various types of materials have been introduced as ER materials, such as polymer/inorganic hybrid materials and the hollow structured materials.[19-23]

Among these various materials, the hollow structured materials have recently received considerable attention from researchers because of theirs high polarization force and high dispersity, which enables the ER fluids to exhibit high performance. For instance, Sung et al. employed polyaniline hollow particles with low-density as an ER material to reduce the sedimentation problem.[24] Cheng et al. improved the ER performance of hollow structures with a large surface area by growing a TiO_2 branch on the TiO_2 hollow sphere.[25] Recently, Jang et al. adopted double-shell SiO_2/TiO_2 hollow nanoparticles as dispersing materials for electrorheological (ER) fluids and found that the ER property significantly enhanced by increasing the number of shells.[26] Although many hollow structured materials as ER disperse phase have been proposed, the influence of hollow structure on ER performance is still ambiguous. Therefore, thorough research is required to clarify the influence of hollow structure on ER activities for a better understanding of the mechanism underlying the ER effect.

Herein, SiO_2/TiO_2 yolk-shell nanospheres (YSNS) with different size of SiO_2 core were simply obtained by etching

[a] Laboratory of Functional and Biological Nanomaterials, College of Materials Science and Engineering, Qingdao University of Science and Technology, Qingdao, China. E-mail: clx@qust.edu.cn

Electronic Supplementary Information (ESI) available: [details of any supplementary information available should be included here]. See DOI: 10.1039/x0xx00000x

method to obtain gradual structural change from yore-shell to hollow structure for studying the influence of structural change of disperse particles on the ER activity. The dielectric parameters of YSNS-based ER fluids were investigated in order to gain further insight into the relationship between structural change and the ER activity. Furthermore, the anti-sedimentation property of the prepared ER fluids was also measured. The relationships between particle density, anti-sedimentation property, dielectric properties and ER behavior were analyzed.

Experimental

Materials

Ethyl silicate (TEOS, 28%) was purchased from Tianjing Bodi Chemical Industry Co.Ltd of China, Ammonia solution (NH_3, 25-28%) and Ethylalcohol (99.7%) were purchased from Laiyang Fine Chemical Plant of China , Hydroxypropyl cellulose (HPC, M_w=100000) was purchased from Alfa Aeser. Titanium tebrabutyl titanate(TBOT, 98%) was purchased from Jiangshu Qiangshen Functional chemical co., LTD of China), Sodium hydroxide (NaOH, 96%), hydrochloricacid (HCl, 96%) and Polydimethyl siloxane fluid (viscosity (η) = (486.5±24.3) mPa·s, and specific density (ρ) = 0.966-0.974 g·cm^{-3} at 25 °C) were purchased from Tianjing Damao Chemical Reagent Factory of China. Low-Density Polyethylene (LDPE) were purchased from Borealis. All of the reagents were used as received, without further purification.

Synthesis of Controllable SiO_2 Template

Colloidal silica templates were prepared through a modified Stöber method.[27] Briefly, Tetraethyl orthosilicate (2 mL) was mixed with the de-ionized water (9 mL), ethanol (80 mL) and an aqueous solution of ammonia (28%, 7 mL). After stirring at 40 °C for 24 h, the white precipitate was obtained by centrifugation, followed by washing with water and ethanol three times, and then dried at 80 °C for overnight.

Preparation of the SiO_2/TiO_2 Core-Shell Nanosphere

The above silica particles were well dispersed in a mixture of hydroxypropyl cellulose (HPC, 0.3 g), ethanol (100 mL) and de-ionized water (0.48 mL) by ultrasonic treatment to get a uniform solution. After stirring for 30 min, tetrabutyl titanate (TBOT, 4 mL) in 20 mL of ethanol was added slowly to the mixture. After injection, the temperature was increased to 85 °C at 900 rpm stirring under refluxing conditions for 100 min. The precipitate was isolated by centrifugation, washed with ethanol, dried at 100 °C for 4 h.

Preparation of SiO_2/TiO_2 York-Shell Nanosphere

The above core/shell composite products were re-dispersed in 80 mL of water under sonication. Then, different amounts of 2.5 M NaOH solution were added and stirred for 6 h at 50 °C for partly removing the silica core to obtain york-shell nanoarchitecture. The YSNS products were isolated by centrifugation, washed with de-ionized water and ethanol, dried under vacuum, dispersed in de-ionized water (150 mg/10 mL), mixed with an aqueous HCl solution, and stirred for 2 h. The resulting precipitates were finally isolated by centrifugation and washed 3 times with de-ionized water, dried at 100 °C for overnight.

Preparation of YSNS-4/LDPE Composite

LDPE and YSNS-4 particles were dried for 8 h at 80 °C and 100 °C, respectively, before melt compounding. LDPE pellets and were melt-blended at 110 °C and 65 rpm for 3 min, using a two-roller mixer (RM-200C, HAPRO Rheometer). Then, YSNS-4 particles and LDPE (weight ratio=1:9) were mixed under strenuous stirring for 7 min. The obtained YSNS-4/LDPE composite was inserted between two steel boards (150 mm×150 mm×2.2 mm) and molded to a 1 mm-thick sheet (sample) by the hot-press method (25T/50T). The hot-press was performed at 10 MPa and 150 °C for 3 min. The sample under the steel boards was cooled in air after the hot-press. The cooling time from 150 °C to room temperature was 45 min.

Characterization

The XRD analysis (Rigaku D/MAX-2500/PC diffractometer) was performed with Cu-Kα irradiation (λ = 1.54178 Å). The surface morphology of the particles was observed by field-emission scanning electron microscopy (FESEM, JEOL JSM-6700F). Transmission electron microscopy (TEM) measurement was observed on a JEOL JEM-2100F instrument with 200 kV accelerated voltage. The dielectric property was measured by broad band dielectric spectroscopy equipment (Novocontrol Concept 40).

Investigation of Electrorheological (ER) Properties

The ER suspensions of the YSNS in silicone oil were obtained as follows: The obtained york-shell nanospheres were dried in a vacuum oven at 80 °C for 12 h. The dried particles were then dispersed in silicone oil [Tian Jin Bodi chemical limited company, Tian Jin, China; dielectric constant (ε) = 2.72-2.78, viscosity (η) = (486.5±24.3) mPa·s, and specific density (ρ) = 0.966-0.974 g·cm^{-3} at 25 °C] to form the ER fluids (10 wt% particle concentration). The concentration of the ER fluids was denoted as the ratio of the nanoparticle weight to the total weight of the ER fluid. Finally, the obtained ER fluids were further heated at 80 °C for 12 h to remove residual water, which may influence the ER behavior. The ER properties of the suspensions were measured by an electrorheometer (HAAKE Rheo Stress 6000, Thermo Scientific, Germany) with a parallel-plate system (PP ER35), and a WYZ-020 DC highvoltage generator (0-5 kV, 0-1 mA). The gap distance between two plates was 1.00 mm and the ER fluid was placed in that space. The steady-flow curves of shear stress-shear rate were measured by the controlled shear rate (CSR) mode at room temperature.

Results and Discussion

Template-mediated syntheses were utilized to synthesize SiO_2/TiO_2 york-shell nanostructures.[28] Synthesis of these materials typically follows several sequential steps (Fig. 1): (i) preparation of the SiO_2 template; (ii) depositing the nanoscale TiO_2 shell layers by slow hydrolysis-condensation kinetics using a sol-gel precursor to form the core-shell nanosphere (CSNS); (iii) amorphous SiO_2/TiO_2 YSNS were obtained by partially etching the silica with NaOH. The size of SiO_2 core could be modified through varying the amount of NaOH.

Structure and morphology

The size, distribution and microstructure of the SiO_2, SiO_2/TiO_2 CSNS and SiO_2/TiO_2 YSNS were determined by SEM (Fig. 2). The SiO_2 particles prepared by the Stoeber method in this work were spherical and smooth as shown in Fig. 2a with mean particle size of 190 nm. In contrast, after coating with an additional layer of the titania, the surfaces of nanospheres became relatively rough and textured, and the size of particles slightly increased (Fig. 2b), indicating that the formation of core-shell structured SiO_2/TiO_2 nanocomposites. It can be seen from Fig. 2c that the structural integrity of the shell maintained well after etching with 3 mL 2.5 M NaOH solution. The insert of Fig. 2c shows formation of voids at the interface of the shell layer, demonstrating that the silica core was etched.

For studying the formation process of the YSNS, the morphology and microstructure of the york-shell products were also characterized by TEM analysis as shown in Fig. 3. All YSNS showed a spherical form, good dispersity and narrow size distribution after chemical etching of the SiO_2 templates. The size of SiO_2 core could be controlled by varying the amount of NaOH. Fig. 3a shows the TEM image of the obtained product with ~164 nm silica core which was etched with 1 mL NaOH solution (denoted as YSNS-1), indicating the dissolution of the SiO_2 core. During the etching process in the alkaline solution, a prior etching process preferentially occured at the SiO_2-TiO_2 interface of SiO_2/TiO_2 CSNS due to the different etching behaviors of silica and titania. When the amount of the added NaOH increased to 2 and 3 mL, respectively, more silica were gradually dissolved during the etching process, generating typical yolk-shell structure shown in Fig. 3b, c (denoted as YSNS-2 and YSNS-3). From the TEM image, it was also concluded that the silica core size of YSNS-2 and YSNS-3 was 142 nm and 114 nm, respectively. Eventually, as the amount of added NaOH solution increased to 4 mL, the SiO_2 core was totally dissolved and hollow nanospheres with ~12 nm titania shell thickness was formed, which is clearly seen in Fig. 3d (denoted as YSNS-4).

Fig. 4 shows the X-ray diffraction patterns of the synthesized YSNS with different size core. No characteristic peak was detected, indicating that both the SiO_2 and TiO_2 were amorphous. The broad peak around 23° gradually shifted to 26° (the broad peak of amorphous TiO_2) with increasing the amount of NaOH solution, which was attributed to the decrease of silica content in SiO_2/TiO_2 composites. With the increasing content of titania, the broad peak of amorphous TiO_2 at 26° became more prominent. These results were consistent with TEM analysis.

Rheological behavior of ER fluids

In order to investigate the influence of the gradual structural change of YSNS on ER performances, the various YSNS-based ER fluids were prepared by dispersing the dried YSNS particles in silicone oil. The flow curves shear-stress as function of shear rate under various electric fields for YSNS with different SiO_2 core size based ER fluids are plotted in Fig. 5. Without an electric field, the shear stress of all ER fluids almost enhanced linearly with increasing shear rate and the slope was near 1, which behaved like a Newtonian fluid.[29-30] While external electric fields were applied, a dramatic increase in the shear stress was observed and each suspension exhibited a plateau in the low-shear-rate region, demonstrating the formation of a chainlike structure among the polarized particles and showed typical characteristics of Bingham fluid behavior.[31-33] As the electric field strength increased, the values of shear stress increased due to the increase in electric field-induced interactions of particles.

Although all suspensions showed ER effects, the difference between them was significant. The ER performance of the YSNS-based ER fluid prominently enhanced with decreasing the SiO_2 core size and the suspension of YSNS-4 represented the highest shear stress under the same electric field strength. For instance, at 3.0 kV mm^{-1} and 1.0 s^{-1}, the shear stress of YSNS-4 suspension was 432 Pa, which was twice higher than that of the YSNS-3 suspension, eight times larger than that of YSNS-2 suspension and 15 times as large as that of YSNS-1 suspension, respectively. At 3.0 kV mm^{-1} and 100 s^{-1}, the shear stress of YSNS-1, YSNS-2, YSNS-3 and YSNs-4 based ER fluid was 121 Pa, 170 Pa, 311 Pa and 609 Pa, respectively. Besides shear stress, ER efficiency is another parameter for evaluating the change in ER behavior of fluids. The ER efficiency can be defined as $[(\tau_E - \tau_0)/\tau_0]$, in which τ_0 is the shear stress under zero electric field strength and τ_E is the shear stress under different external electric field strengths.[34] Here, at 3 kV mm^{-1} and 1.0 s^{-1}, the ER efficiency for the suspension of YSNSs-1, YSNSs-2, YSNSs-3 and YSNSs-4 was 3.2, 5.1, 20.6 and 57.9, respectively. All these results showed that the ER performance of the YSNS-based ER fluid prominently enhanced with decreasing the SiO_2 core size, which were attributed to the increase of electric field force between the polarized YSNS. The reason will be further analyzed below.

It was also found in Fig. 5 that the shear stress decreased to a minimum value as a function of shear rate after the appearance of a maximum value and then climbed with the increase of shear rate, indicating that the electric field-induced electrostatic interaction between YSNS could not overcome the shear field-induced hydrodynamic interaction with increasing shear rate and, as a consequence, the broken particle chains were not able to completely rebuild.[35-36] Moreover, the shear rate, at which the maximum shear stress was obtained (arrows in Fig. 5, denoted as $\dot{\gamma}_{mss}$), increased with the electric field strength.[37] As the electric field strength

increased, the electric field-induced electrostatic interaction between microspheres was enhanced. Therefore, a relative high shear rate was required to promote hydrodynamic interaction in order to break particle chains. Meanwhile, it could be found that under the same electric field strength, the value of $\dot{\gamma}_{mss}$ increased with the decrease of silica core size, which also confirmed that the electric field-induced electrostatic interaction between nanospheres was enhanced with decreasing the size of SiO_2 core. As shown in Fig. 5d, the stable flow curve and the widest plateau level of shear stress versus shear rate reflected that the electric field-induced electrostatic interaction between YSNS-4 was so strong that it could effectively rebuild particle chains in the wide shear rate range. The stable flow curves in a wide shear rate region are useful for technological applications. Shear viscosities of various YSNS-based fluids were also evaluated as the function of shear rate (Fig. S1). It was confirmed that various YSNS-based ER fluids showed typical shear thinning behavior with increasing shear rate.[38-39]

Dielectric property of ER fluids

To gain more insight into the dependence of ER activity with dielectric property, the permittivity (ε') were investigated by broadband dielectric spectroscopy (Fig. 6). Previous studies have reported that the large $\Delta\varepsilon'$ in the frequency range of 10^2-10^5 Hz ($\Delta\varepsilon'_{100Hz\text{-}100kHz}$) indicated strong polarizability at the interface between disperse particles and silicone oil, which had a positive influence on the ER performance. Usually, $\Delta\varepsilon'_{100Hz\text{-}100kHz}$ were obtained by two ways: (i) $\Delta\varepsilon' = \varepsilon'_{100Hz} - \varepsilon'_{100kHz}$ (ε'_{100Hz} and ε'_{100kHz} is the value of ε' corresponding to the frequency of 10^2 Hz and 10^5 Hz, respectively).[40-41] (ii) The dielectric spectra data (10^2-10^5 Hz) are fit using Cole-Cole equation:[42]

$$\varepsilon^* = \varepsilon' + i\varepsilon'' = \varepsilon'_\infty + \frac{\varepsilon'_0 - \varepsilon'_\infty}{1 + (i\omega\tau)^{1-\alpha}}$$

where ε_0 is the dielectric constant of an ER fluid at the low frequency limit, ε_∞ is the dielectric constant of an ER fluid at the high-frequency limit and ε'_0-ε'_∞ reflects the achievable dielectric polarizability.

Determined achievable polarizability $\Delta\varepsilon'_{(100Hz\text{-}100kHz)}$ for YSNS-1, YSNS-2, YSNS-3 and YSNS-4 based ER fluids were 0.34, 0.67, 1.01 and 0.93, respectively. The highest polarizability of YSNS-3 based ER fluid implied that it should have the largest electrostatic interaction and provide the highest yield stress, which were different to the results of ER performance. Therefore, using the value of $\Delta\varepsilon'_{100Hz\text{-}100kHz}$ to appraise the polarization of the particles in ER fluid was flawed, which was caused by the negligence of distributing change of polarized disperse particles in ER fluid. The mechanism will be further analyzed below.

It is well-known that the intensity of electric field for dielectric test is much lower than that used in the ER test. As a result, compared with the ER test, the mobility of polarized particles in the dielectric test process is relative low. Hence, the influence of distributing change of disperse particles in ER fluid on the polarization of particles is more easily monitored by the dielectric test, which can be embodied by the variation of permittivity. Fig. 7 shows schematic illustration for the relationship between permittivity and polarization behavior of YSNS-4 in ER fluid. It can be seen from Fig. 7a that there was no interface polarization in the ER fluid occurred without an electric field. When the electric field was applied, the dispersed particles were polarized instantly. At high-frequency, there was not enough time for the polarized particles to transfer to another location. As a result, the distribution of particles still kept the original disorder state (Fig. 7b). Compared with high-frequency, at the low frequency, the polarized particles had relatively long time to form the chain-like structures along the electric field direction. The structural evolution from disorder to relative order in the ER fluid would reduce the polarized particles distance (d_P) along the electric field direction, which further induced secondary polarization and the increase of polarized charge (seen in Fig. 7c). The increase of polarized charges could further result in the enhancement of permittivity. Consequently, the permittivity of ER fluid was closely related to the distribution of polarized disperse particles in ER fluid.

While a strong DC electric field was applied, the dispersed particles in ER fluid could translocate to form the chain-like structures immediately, resulting in further increase of the permittivity of the ER fluid. As a consequence, it could be deduced that $\Delta\varepsilon'_{0.01Hz\text{-}100kHz}$ obtained in the frequency range of 10^{-2}-10^5 Hz was more suitable for analyzing the polarizability of ER system. At low shear rates, the hydrodynamic interaction was so small that it was unable to overcome the interparticle electrostatic interaction and, as a result, the particle chains could be well maintained and the suspension approximately behaved as an elastic solid. While the shear rate increased continually, the shear field-induced hydrodynamic interaction would start to destroy the particle chains, resulting in the increase of average distance between polarized particles along the electric field direction. The polarized charges at the interface of particles due to secondary polarization (P_{sp}) decreased with the increase of d_P, which induced the decrease of electrostatic interaction between particles. Consequently, the suspension displayed a maximum value of shear stress and a plateau level of shear stress versus shear rate corresponding to a balanced situation where the particle chains are continuously broken and rebuilt by competition between electrostatic interaction and hydrodynamic interaction. At high shear rates, the destruction of particle chains became more serious and the average distance between polarized particles would further increase, inducing significant reduction of the P_{sp}. As a result, the effect of electrostatic interaction significantly decreased with the increase of d_P and the hydrodynamic interaction dominated the fluid flow. This phenomenon was called shear-thinning behavior.

In order to further demonstrate that the distributing change of disperse particles in ER fluid from disorder to relative order in the ER fluid would induce the enhancement of permittivity at the low frequency, the YSNS-4/Low-Density Polyethylene (LDPE) solid composite in which the disperse YSNS remained

stationary and stayed in the disordered state was prepared. The dielectric spectroscopy of LDPE and YSNS-4/LDPE composite was shown in Fig. 8a. The permittivity of LDPE exhibited almost no variation with frequency in the 10^{-2}-10^{5} Hz. Compared with LDPE, the permittivity of YSNS-4/LDPE composite increased with the decrease of frequency in the range of 10^{2}-10^{5} Hz, which was due to the interface polarization, and no further enhancement of the permittivity was observed in the low frequency range of 10^{-2}-10^{0} Hz. Interestingly, unlike YSNS-4/LDPE composites, the permittivity curves of the YSNS-4 based ER fluid showed a significant enhancement in 10^{-2}-10^{0} Hz. Therefore, it could be further concluded that the enhancement of the permittivity of the YSNS-4 based ER in the low frequency (10^{-2}-10^{0} Hz) was due to the distributing change of disperse particles in ER fluid from disorder to relative order.

In conclusion, the value of $\Delta\varepsilon'$ (ε'_{100Hz}-ε'_{100kHz} or ε'_{0}-ε'_{∞} obtained from Cole-Cole equation) which is usually used to characterize the value of achievable polarizability just demonstrated the instant intensity of the interface polarization in the ER fluid which reflected the immediate response of materials to electric field. If the dispersed particles remained static in the silicone oil, the value of $\Delta\varepsilon'_{(100Hz\text{-}100kHz)}$ could represent the polarization of the ER fluid. However, in ER fluid-system, the dispersed particles in ER fluid could trend to form the chain-like structures immediately. As a consequence, it could be deduced that $\Delta\varepsilon'_{(0.01Hz\text{-}100kHz)}$ obtained in the frequency range of 10^{-2}-10^{5} Hz should more accurate for analysing polarizability in the system of ER fluid. The polarizability $\Delta\varepsilon'_{(0.01Hz\text{-}100kHz)}$ and other physical parameters for various YSNS-based ER fluids was listed in Table 1. The $\Delta\varepsilon'_{(0.01Hz\text{-}100kHz)}$ of YSNS based ER fluid enhanced with decreasing the SiO_2 core size, which implied that YSNS with smaller SiO_2 core based ER fluid should have more number of P_{sp}. Furthermore, the increase of P_{sp} would induce the enhancement of electric field-induced electrostatic interaction between particles. Hence, the YSNS with smaller SiO_2 core based ER fluid showed the larger shear stress at the same testing condition.

Through the above analysis, it could be concluded that the P_{sp} took an important role in the ER performance. The number of P_{sp} was close related to the distribution of dispersed particles in ER fluid. Thus, the ability to maintain the chain-like structure was significantly important for ER system and a method to characterize the ability should be required.

When dielectric spectroscopy equipment tested the data point at 10^{-2} Hz, the period of the alternating electric field was 100 s. Thus, it could be concluded that the direction of the external electric field would remain unchanged in 50 s, which was more than the relaxation time of interface polarization. After interface polarization completed, the polarized particles had long time to translocate to form the chain-like structures. While electric field direction changed, the surface polarity of dispersed particles reversed immediately. The dispersed particles would continue to form the chain-like structures based on the previous half-cycle of the alternating electric field rather than come back to a disorder state, which was due to the viscosity of the medium. Thus, the behavior of dispersed particles in low frequency dielectric test was similar to the electrorheological behavior under DC electric field. Furthermore, the characteristic of permittivity curve in the low frequency range could reflect the distribution change of polarized particles in the medium. Herein, the parameter K was used to quantify the absolute value of slope of permittivity curves at 10^{-2} Hz (Fig. 8b), which indicated the increment of permittivity per unit time. The increase of permittivity in the low frequency range was attributed to structural evolution from disorder to relative order. The permittivity curves of ER fluid with a larger K indicated that the ER fluid had higher efficiency of structural evolution. Consequently, the value of K could reflect the efficiency of order-to-disorder transition of dispersed particles in silicone oil. The values of K for various YSNS-based ER fluids were described in Table 1. It can be seen that the smaller SiO_2 core-YSNS based ER fluid exhibited higher value of K, which was associated with higher efficiency of structural evolution. It is well known that the rheological behaviour of ER fluids is dominated by the completion between the electric field-induced electrostatic interaction between particles and the shear field-induced hydrodynamic interaction, which is a dynamic balancing state (breaking and rebuilding of particle chain structures). Thus, the ER fluid with higher value of K had a better structural recoverability to maintain the chain-like structures, which implied that the number of P_{sp} was more than the others, resulting in a larger dynamic yield stress (seen in Fig. S2) and a wider plateau level of shear stress versus shear rate.

Additionally, it could be concluded that the polarizability $\Delta\varepsilon'_{(100Hz\text{-}100kHz)}$ of YSNS-3-based ER fluid was higher than that of YSNS-4, which might be caused by the excessive etching, just indicating that the instant electrostatic interaction of YSNS-3 was larger than YSNS-4 while the electric field was applied. Thus, at this moment, the YSNS-3 based ER should have a higher efficiency of structural evolution than YSNS-4 based ER, which seemed to contradict with the dielectric results ($K_{YSNS\text{-}4}$>$K_{YSNS\text{-}3}$). In fact, YSNS-4 had a relative lower density (shown in the Table 1) so that the mass of individual particles was smaller. Though the YSNS-3 had larger electrostatic interaction, it was possible for YSNS-4 to have a higher efficiency of structural evolution because of its larger mobility. As a result, the permittivity of the YSNS-4 based ER fluid exceeded that of the YSNS-3 based ER fluid at the low frequency (dashed circle shown in Fig. 6), which was attributed to higher efficiency of structural evolution of YSNS-4 based ER fluid.

The schematic illustration for explanation on the effect of YSNS with different core size on electrostatic interaction was provided in Fig. 9. When an external electric field was applied in the ER fluid, the polarized particles formed a fibrillar structure along the electric field direction. Meanwhile, the mass of YSNS decreased with the SiO_2 core size. As a result, the number of YSNS with smaller SiO_2 core dispersed in ER fluid (10 wt% particle concentration) is larger than that of YSNS with larger one, resulting in smaller d_p and more number of particle chains. For YSNS based ER system, the influence of polarization

behavior of SiO_2 core on global polarization of the ER fluid was ignored, attributing to two reasons. One reason was that under an applied DC electric field, the electric field inside the TiO_2 shell was shielded by the interfacial polarization of TiO_2 shell, which resulted in weak polarization of SiO_2 core. The other reason is that the permittivity of SiO_2 was much lower than that of TiO_2. The interfacial charge on the surface of SiO_2 core which was caused by polarization could not affect the polarization of the TiO_2 shell. Therefore, the polarization of TiO_2 shell played more important role in electrostatic interaction than polarization of SiO_2 core. Combining the above analysis, the YSNS with smaller SiO_2 core should have more number of P_{sp} because of its smaller d_p, resulting in the YSNS with smaller SiO_2 core should had larger electrostatic interaction. Consequently, the YSNS with smaller SiO_2 core based ER fluid represented higher shear stress, which was ascribed to the larger polarization force and more number of particle chains. Once the shear rate increased to some extent, shear field-induced hydrodynamic interaction would destroy particle chains, which induced the increase of average distance between polarized particles along the electric field direction. As a result of its higher efficiency of structural evolution, the YSNS with smaller SiO_2 core based ER fluid had a better ability to maintain the chain-like structure, which was associated with smaller average d_p and more number of P_{sp}. Hence, in the shearing process, the electrostatic interaction between YSNS increased with the size of SiO_2 core and the YSNS-4 based ER fluid displayed the largest dynamic yield stress and widest plateau level.

The sedimentation ratio test at room temperature was used to characterize the suspended stability of ER fluid.[43] In order to accelerate the settling velocity, ethanol was chosen as the dispersing medium. The sedimentation ratio was defined by the height percentage of the particle-rich phase relative to the total suspension height. From Fig. 10, it could be seen that the anti-settling property was improved as the diameter of SiO_2 core decreased. The YSNS-4 exhibited an outstanding anti-sedimentation property because of its relative low density and the sedimentation ratio was maintained above 0.63 even after 15 days.

Conclusions

YSNS had been successfully synthesized via a conventional templating method which combined sol-gel coating and partial etching processes. The influence of gradual structural change of disperse particles on ER properties was examined. The rheological results showed that the ER properties of YSNS suspensions improved as the size of silica core decreased and the hollow TiO_2-based ER fluid represented highest yield stress. The improvement of ER activities was contributed to the enhancement of polarization force between particles. The YSNS with smaller SiO_2 core based ER fluid had the smaller distance between the polarized particles (d_p) and more number of particle chains. Thus, the polarized charges at the interface of particles due to secondary polarization (P_{sp}) increased with the decrease of d_p, which could be concluded that the smaller d_p could induce the largest polarization force because of more number of P_{sp}. Consequently, at the beginning of the shearing process, the YSNS with smaller SiO_2 core based ER fluid exhibited larger yield stress. At low shear rate, the ability of ER fluid to maintain the chain-like structure was closely related to the number of P_{sp}, which could be evaluated by the absolute value of slope of permittivity curves (K). The YSNS with smaller SiO_2 core based ER fluid had a better ability to maintain the chain-like structures, resulting in more number of P_{sp}. Therefore, the YSNS with smaller SiO_2 core based ER fluid should have a larger dynamic yield stress and a wider plateau level. Meanwhile, it was found that the value of $\Delta\varepsilon'_{(100Hz\text{-}100kHz)}$ just demonstrated the initial intensity of the interface polarization in the ER fluid as the electric field was applied and the polarizability $\Delta\varepsilon'_{(0.01Hz\text{-}100kHz)}$ obtained in the frequency range of 10^{-2}-10^{5} Hz was more suitable for analyzing the system of ER fluid, which was attributed to structural evolution of polarized particles in ER fluid. The result was important in expanding the application of the dielectric spectrum in the field of ER.

Acknowledgements

This work is supported by National Natural Science Foundation of China (no. 51407098), Natural Science Foundation of Shandong Province of China (ZR2014EEM006), the Science-Technology Foundation for Middle aged and Young Scientist of Shandong Province, China (no. BS2014CL018), Development Program in Science and Technology of Qingdao (no. 14-2-4-50-jch), A Project of Shandong Province Higher Educational Science and Technology Program (no. J14LA14).

References

1 T. Hao, *Adv. Mater.*, 2001, ***13***, 1847-1857.
2 T. C. Halsey, *Science*, 1992, ***258***, 761-766.
3 W. J. Wen, X. X. Huang, S. H. Yang and K. Q. Lu, *Nat. Mater.*, 2003, ***2***, 727-730.
4 L. Y. Liu, X. X. Huang, C. Shen, Z. Y. Liu, J. Shi, W. J. Wen and P. Sheng, *Appl. Phys. Lett.*, 2005, ***87***, 104106-1-3.
5 M. Grzelczak, J. Vermant, E. M. Furst and L. M. Liz-Marzán, *ACS Nano*, 2010, ***4***, 3591-3605.
6 K. Negita, Y. Misono, T. Yamaguchi and J. Shinagawa, *J. Colloid Interface Sci.*, 2008, ***321***, 452-458.
7 W. L. Zhang, Y. D. Liu, H. J. Choi and S. G. Kim, *ACS Appl. Mater. Interfaces*, 2012, ***4***, 2267-2272.
8 W. Wen, X. Huang and P. Sheng, *Soft Matter*, 2008, ***4***, 200-210.
9 J. Y. Hong and J. Jang, *Soft Matter*, 2010, ***6***, 4669-4671.
10 J. Y. Hong, E. Lee and J. Jang, *J. Mater. Chem. A*, 2013, ***1***, 117-121.
11 Y. M. Han, P. S. Kang, K. G. Sung and S. B. Choi, *J. Intell. Mater. Syst. Struct.*, 2007, ***18(12)***, 1149-1154.
12 S. Z. Ma, F. H. Liao, S. X. Li, M. Y. Xu, J. R. Li, S.H. Zhang, S. M. Chen, R. L. Huang and S. Gao, *J. Mater. Chem.*, 2003, ***13***, 3096-3102.
13 P. Tan, W. J. Tian, X. F. Wu, J. Y. Huang, L. W. Zhou and J. P. Huang, *J. Phys. Chem. B.*, 2009, ***113*** **(27)**, 9092-9097.
14 S. Chen, X. Huang, N. F. Van der Vegt, W. Wen and P Sheng, *Phys. Rev. Lett.*, 2010, ***105(4)***, 046001-1-4.
15 J. B. Yin and X. P. Zhao, *Chem. Mater.*, 2004, ***16***, 321-328.

16 T. Plachy, M. Mrlik, Z. Kozakova, P. Suly, M. Sedlacik, V. Pavlinek and I. Kuritka, *ACS Appl. Mater. Interfaces*, 2015, ***7(6)***, 3725-3731.
17 K. Tang, Y. L. Shang, J. R. Li, J. Wang and S. H. Zhang, *J. Alloy Compd.*, 2006, ***418***, 111-115.
18 M. Sedlacik, M. Mrlik, Z. Kozakova, V. Pavlinek and I. Kuritka, *Colloid Polym. Sci.*, 2013, ***291(5)***, 1105-1111.
19 H. Hu, X. Wang, J. Wang, F. Liu, M. Zhang and C. Xu, *Appl. Surf. Sci.*, 2011, ***257***, 2637-2642.
20 R. Shen, X. Z. Wang, Y. Lu, D. Wang, G. Sun, Z. X. Cao and K. Q. Lu, *Adv. Mater.*, 2009, ***21***, 4631-4635.
21 Y. C. Cheng, X. H. Liu, J. J. Guo, F. H. Liu, Z. X. Li, G. J. Xu and P. Cui, *Nanotechnology*, 2009, ***20***, 055604-1-7.
22 J. B. Yin, X. A. Xia, L. Q. Xiang and X. P. Zhao, *J. Mater. Chem.*, 2010, ***20***, 7096-7099.
23 J. H. Wu, F. H. Liu, J. J. Guo, P. Cui, G. J. Xu and Y. C. Cheng, *Colloids and Surfaces A: Physicochem. Eng. Aspects.*, 2012, ***410***, 136-143.
24 B. H. Sung, U. S. Choi, H. G. Jang and Y. S. Park, *Colloids Surf. A*, 2006, ***274***, 37-42.
25 Q. Cheng, V. Pavlinek, Y. He, Y. Yan, C. Li and P. Saha, *Colloid Polym. Sci.*, 2011, ***289***, 799-805.
26 S. G. Lee, J. S. Lee, S. H. Hwang, J. Y. Yun and J. Jang, *ACS Nano*, 2015, ***9***, 4939-4949.
27 W. Stöber, A. Fink and E. Bohn, *J. Colloid Interface Sci.* 1968, ***26***, 62-69.
28 J. B. Joo, I. Lee, M. Dahl, G. D. Moon, F. Zaera and Y. D. Yin, *Adv. Funct. Mater.*, 2013, ***23***, 4246-4254.
29 K. Y. Shin, S. Lee, S. Hong and J. Jang, *ACS Appl. Mater. Interfaces*, 2014, ***6***, 5531-5537.
30 I. S. Sim, J. W. Kim, H. J. Choi, C. A. Kim and M. S. Jhon, *Chem. Mater.*, 2001, ***13***, 1243-1247.
31 T. C. Halsey, *Adv. Mater.* 1993, ***5***, 711-718.
32 J. Y. Hong, M. Choi, C. Kim and J. Jang, *J. Colloid Interface Sci.* 2010, ***347***, 177-182.
33 Y. Z. Dong, J. B. Yin and X. P. Zhao, *J. Mater. Chem. A*, 2014, ***2***, 9812-9819.
34 J. B. Yin, Y. J. Shui, Y. Z. Dong and X. P. Zhao, *Nanotechnology,* 2014, ***25***, 045702-1-11.
35 M. S. Cho, J. W. Kim, H. J. Choi and M. S. Jhon, *Polym. Adv.Technol.*, 2005, ***16***, 352-356.
36 Y. Y. Song, H. Hildebrand and P. Schmuki, *Surf. Sci.*, 2010, ***604***, 346-353.
37 J. Y. Hong and J. Jang, *Soft Matter*, 2012, ***8***, 7348-7350.
38 M. Mrlik, M. Sedlacik, V. Pavlinek, P. Bober, M. Trchova, J. Stejskal and P. Saha, *Colloid Polym. Sci.*, 2013, ***291***, 2079-2086.
39 M. Sedlacik, M. Mrlik, V. Pavlinek, P. Saha and O. Quadrat, *Colloid Polym. Sci.*, 2012, ***290***, 41-48.
40 H. Block, J. P. Kelly, A. Qin and T. Wastson, *Langmuir*, 1990, ***6***, 6-14.
41 J. B. Yin and X. P. Zhao, *J. Phys. Chem. B*, 2006, ***110***, 12916-12925.
42 H. J. Choi, C. H. Hong and M. S. Jhon, *Int. J. Mod. Phys. B*, 2007, ***21***, 4974-4980.
43 C. M. Yoon, S. Lee, S. H. Hong and J. Jang, *Journal of Colloid and Interface Science*, 2015, ***438***, 14-21.

Figures

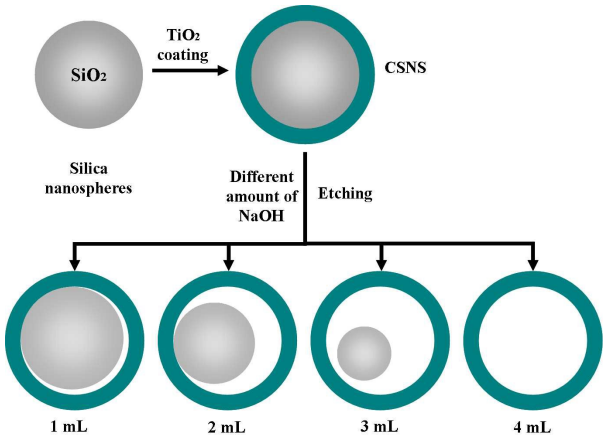

Fig. 1 Schematic illustration showing the general strategy for the synthesis of ST YSNS.

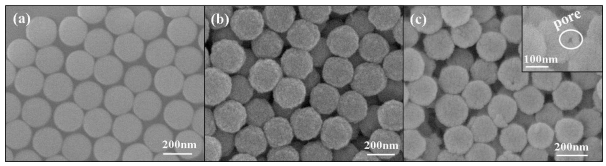

Fig. 2 SEM images of (a) SiO_2 particles; (b) TiO_2-coated SiO_2 nanospheres; (c) SiO_2/TiO_2 YSNS obtained by etching the silica with 3 mL NaOH.

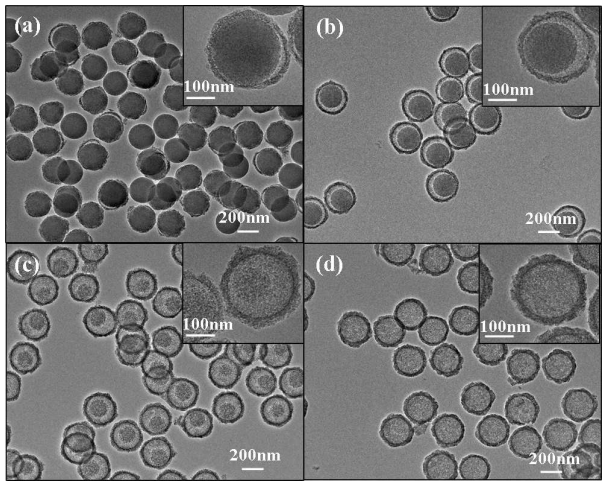

Fig. 3 TEM images show the morphology evolution of SiO_2-TiO_2 york-shell nanospheres after etching at 50 °C for 5 h with different amount of 2.5 M NaOH (a) 1 mL; (b) 2 mL; (c) 3 mL; (d) 4 mL.

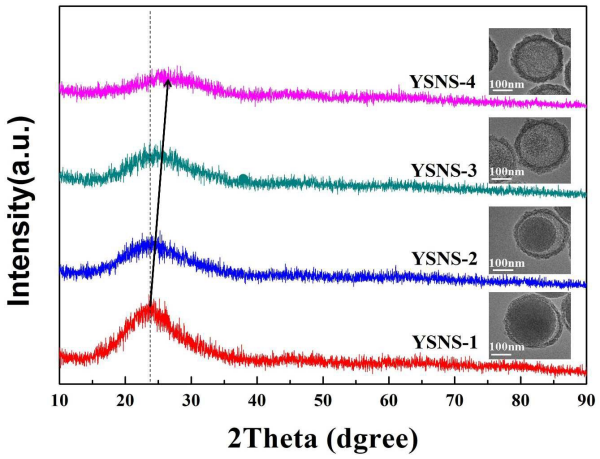

Fig. 4 X-ray diffraction patterns of various YSNS.

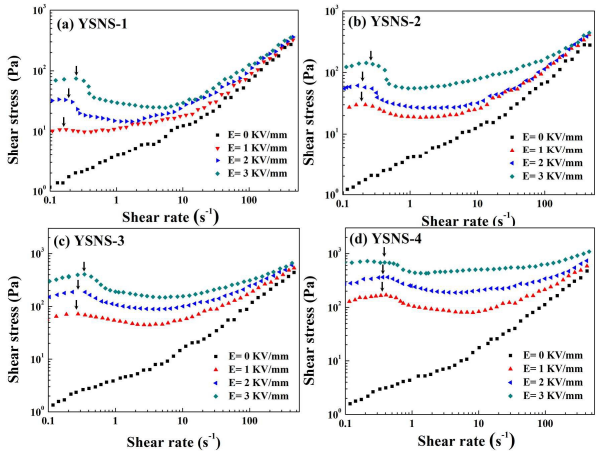

Fig. 5 Shear stress as a function of shear rate under various electric fields (a) YSNS-1; (b) YSNS-2; (c) YSNS-3; (d) YSNS-4 based ER fluids.

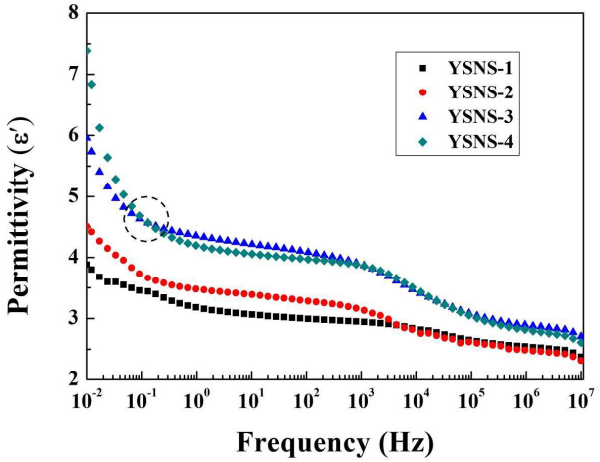

Fig. 6 Permittivity (ε') as a function of electric field frequency for four kinds of YSNS based ER fluids (10 wt% in silicone oil).

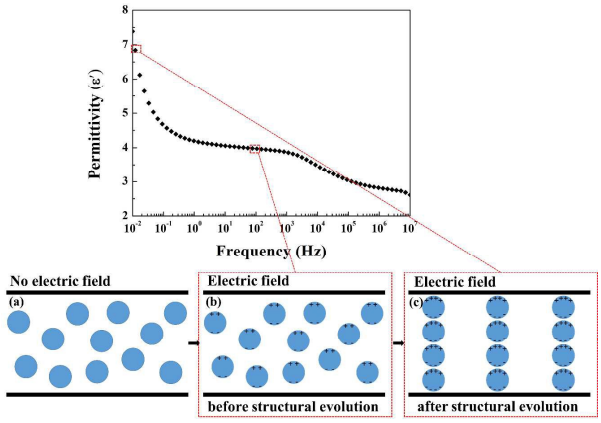

Fig. 7 The schematic illustration for the relationship between permittivity and polarization behavior of YSNS-4 based ER fluid (a) before the dielectric test; (b) during high-frequency dielectric test; (c) during low frequency dielectric test.

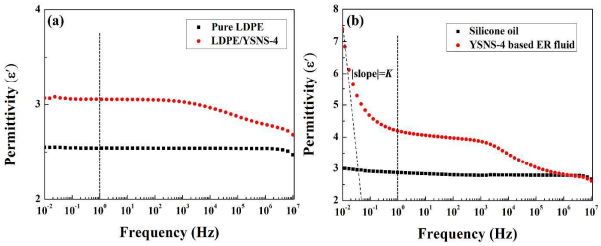

Fig. 8 The permittivity curves of (a) LDPE and YSNS-4/LDPE composite; (b) silicone oil and YSNS-4 based ER fluid.

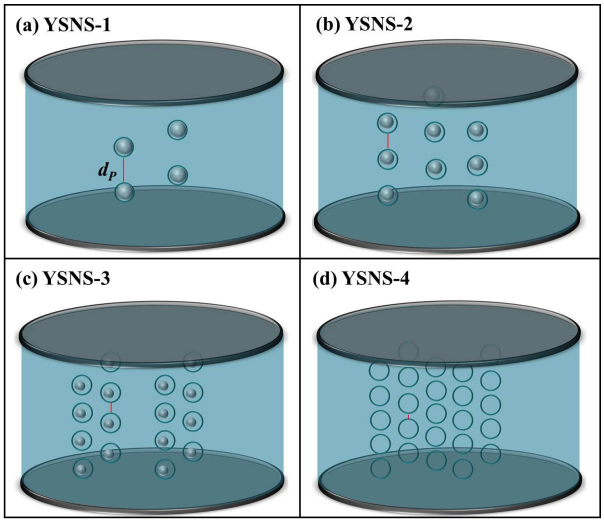

Fig. 9 Schematic illustration showing dispersion of various YSNS in silicone oil between two parallel plates.

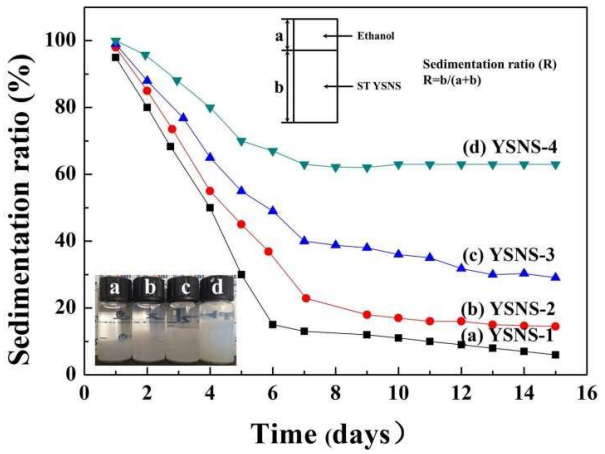

Fig. 10 Sedimentation ratio as a function of ageing time for various YSNS ER fluids at particle concentrations of 10 wt%.

Table

Table 1 The relevant parameters for various YSNS-based ER fluids

Sample	*Particle size (nm)*	*Shell thickness (nm)*	$\varepsilon'_{0.01Hz}$	ε'_{100Hz}	ε'_{100KHz}	$\Delta\varepsilon'_{(100Hz-100KHz)}$	$\Delta\varepsilon'_{(0.01Hz-100KHz)}$	$K_{(0.01Hz)}$	*Density* ($g \cdot cm^{-3}$)
YSNS-1	211	12	3.89	2.99	2.65	0.34	1.24	0.41	2.42
YSNS-2	220	18	4.51	3.29	2.62	0.67	1.89	0.79	2.24
YSNS-3	225	22	6.01	4.08	3.07	1.01	2.94	1.36	2.12
YSNS-4	229	27	7.41	3.98	3.05	0.93	4.36	2.72	1.94